J Therm Anal Calorim (2011) 103:1119–1124
DOI 10.1007/s10973-010-1218-6

Thermodynamic properties and molar heat capacity of $Er_2(Asp)_2(Im)_8(ClO_4)_6{\cdot}10H_2O$

X.-C. Lv · Z.-C. Tan · X.-H. Gao

Received: 24 September 2010 / Accepted: 24 November 2010 / Published online: 14 December 2010

Abstract A complex of Erbium perchloric acid coordinated with L-aspartic acid and imidazole, $Er_2(Asp)_2(Im)_8(ClO_4)_6{\cdot}10H_2O$ was synthesized for the first time. It was characterized by IR and elements analysis. The heat capacity and thermodynamic properties of the complex were studied with an adiabatic calorimeter (AC) from 80 to 390 K and differential scanning calorimetry (DSC) from 100 to 300 K. Glass transition and phase transition were discovered at 220.45 and 246.15 K, respectively. The glass transition was interpreted as a freezing-in phenomenon of the reorientational motion of ClO^{4-} ions and the phase transition was attributed to the orientational order/disorder process of ClO^{4-} ions. The thermodynamic functions $[H_T - H_{298.15}]$ and $[S_T - S_{298.15}]$ were derived in the temperature range from 80 to 390 K with temperature interval of 5 K. Thermal decomposition behavior of the complex in nitrogen atmosphere was studied by thermogravimetric (TG) analysis and differential scanning calorimetry (DSC).

X.-C. Lv · X.-H. Gao
School of Chemistry and Material Science, Liaoning Shihua University, Fushun 113001, China

Z.-C. Tan (✉)
Thermochemistry Laboratory, Dalian Institute of Chemical Physics, Chinese Academy of Science, Dalian 116023, China
e-mail: tzc@dicp.ac.cn

Z.-C. Tan
China Ionic Liquid Laboratory, Dalian Institute of Chemical Physics, Chinese Academy of Science, Dalian 116023, China

Keywords $Er_2(Asp)_2(Im)_8(ClO_4)_6{\cdot}10H_2O$ · Adiabatic calorimetry · Low-temperature heat capacity · Glass transition · Phase transition · Thermal analysis

Introduction

Since in 1975, Anghileri firstly reported that $[La(Gly)_3(H_2O)]Cl_3{\cdot}3H_2O$ has anti-tumor effect [1], the complexes of rare earth ions with amino acids have been studied extensively. Up to now they have been used in many areas for their physiological and biochemical effects, such as fertilizer, pesticide, antibacterial agent and so on. As a result, rare earth elements are inevitably spread into the bodies of beings. In order to obtain information about the long-term effect of rare earth elements on people and explore more extensively application of the complexes, the complexes have been synthesised and studied by a variety of methods [2–6]. However, a few publications deal with thermodynamic properties [7, 8] such as molar heat capacities $C_{p,m}$ of compound at different temperatures, from which many other thermodynamic properties can be calculated for both theoretical and practical purposes.

In the present study, a complex of Erbium perchlorate coordinated with L-aspartic acid and imidazole, $Er_2(Asp)_2(Im)_8(ClO_4)_6{\cdot}10H_2O$, which has never been reported, was synthesized and characterized. The molar heat capacity, $C_{p,m}$, and thermodynamic properties of the complex were studied by the AC and DSC techniques. Two special thermal phenomena were discovered and the mechanism was deduced. The temperature, T_{trs}, molar enthalpies, $\Delta_{trs}H_m$, molar entropies, $\Delta_{trs}S_m$, of the phase transitions and thermodynamic functions, $[H_T - H_{298.15}]$ and $[S_T - S_{298.15}]$ were derived, respectively [9–11]. The mechanism of decomposition of the complex was studied by DSC and TG technique.

Experimental

Synthesis and characterization of the complex

$Er_2(Asp)_2(Im)_8(ClO_4)_6{\cdot}10H_2O$ has never been reported in any other documents we have seen. The starting material was the analytical reagent from the Beijing Chemical Reagent Co. The rare earth oxide (Er_2O_3) was dissolved in an excess amount of perchloric acid, and the concentration of the solution was determined by EDTA titration analysis. Then, solid L-aspartic acid was added to the solution of Er^{3+} in molar ratio of Er^{3+}: Asp = 1:1. After the pH value of the reaction mixture was carefully adjusted to about 4.0 by slow addition of NaOH solution, imidazole was added. The solution was placed in a desiccator filled with phosphorus pentaoxide after a further 2 h of stirring. The complex was obtained about a month later.

An elemental analysis apparatus (Model PE-2400 II, USA) was used to measure the C, H, N of the complex, and Er was determined by EDTA titration. Found: Er (16.481%), C (19.952%), N (13.101%), and H (2.461%), which is close to the theoretical value, Er (17.360%), C (19.544%), N (14.629%), and H (2.694%). The sample formula was determined to be $Er_2(Asp)_2(Im)_8(ClO_4)_6{\cdot}10H_2O$ and the purity, obtained from the EDTA titration under the same conditions was found to be 99.58%.

Infrared spectra of the complex and L-aspartic acid were obtained, KBr pellets at room temperature using a Bruker Tensor 27-IR spectrophotometer. Compared with the IR spectrum of L-aspartic acid, the ν_s (carboxyl) band of the complex shifted from 1,410 cm^{-1} to higher wavenumbers (1,431 cm^{-1}), which shows that the carboxyl groups of the ligand have been coordinated to the metal ion [12]. The special absorptions of $-NH_2$ shifted from 3,050 to 3,240 cm^{-1} (ν_{-NH}), 2,750 to 2,740 cm^{-1} (ν_{-NH}), and 1,560 to 1,562 cm^{-1} (δ_{NH_2+}), because a hydrogen bond formed in the complex. The spectrum also shows the wide peak symmetrical resonance frequencies, ν_s (N–H), shifted from 3,286–3,425 cm^{-1} down to 3,166–3,098 cm^{-1}, which is evidence of the coordination of imidazole molecules [13]. A broad absorption band for ν (hydroxyl) appearing at 3,400 cm^{-1} shows the presence of water molecules in the complex.

Adiabatic calorimetry

A precision automatic adiabatic calorimeter was used to measure the heat capacities of the complex over the temperature range from 80 to 390 K. The instrument was established in Thermochemistry Laboratory of Dalian Institute of Chemical Physics, Chinese Academy of Sciences. The structure and principle of the adiabatic calorimeter have been described in detail elsewhere [14–18].

Prior to the heat capacity measurement of the sample, the molar heat capacities of α-Al_2O_3, the standard reference material, were measured from 78 to 400 K to verify the reliability of the adiabatic calorimeter. The results showed that the deviation of our calibration data from those of NIST [19] was within ±0.3%. In the present article, the mass of $Er_2(Asp)_2(Im)_8(ClO_4)_6{\cdot}10H_2O$ used for the measurement was 1.39251 g.

DSC and TG

A Differential Scanning Calorimeter (DSC-141, SETARAM, France) was used to perform the thermal analysis of $Er_2(Asp)_2(Im)_8(ClO_4)_6{\cdot}10H_2O$ from 100 to 300 K with liquid nitrogen as cryogen and from 300 to 700 K at the heating rate of 10 K min^{-1} under nitrogen. The mass of the sample used in the experiments were 3.37 and 3.80 mg, respectively.

The TG measurement of the sample was carried out by a thermogravimetric analyzer (Model: DT-20B, Shimadzu, Japan) at the heating rate of 10 K min^{-1} under nitrogen, with flow rate of 30 mL min^{-1}. The mass of the sample used in the experiment was 6.9 mg.

Results and discussion

Molar heat capacity, molar enthalpies, and entropies

The experimental molar heat capacities of $Er_2(Asp)_2(Im)_8(ClO_4)_6{\cdot}10H_2O$ from 80 to 390 K are plotted in Fig. 1 and listed in Table 1.

It can be seen from Fig. 1 that there is a slight step at 219.64 K on the $C_{p,m} - T$ curve, which is consistent with the DSC curve (T_{trs} = 220.4 K). Such thermal event was deduced to be the glass transition of the complex. There are

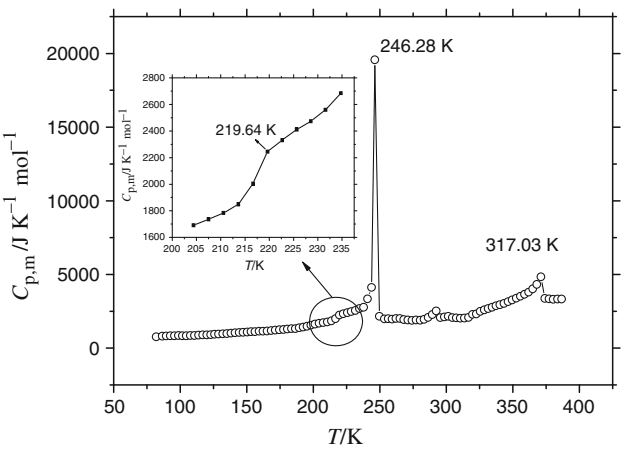

Fig. 1 Experimental molar heat capacities plotted against temperature of the complex as a function of temperature

Table 1 Experimental molar heat capacities of the complex from 80 to 390 K

T/K	$C_{p,m}$/J K^{-1} mol^{-1}	T/K	$C_{p,m}$/J K^{-1} mol^{-1}
81.899	765.01	162.21	1149.6
86.571	808.75	165.20	1168.5
89.444	823.72	168.32	1194.8
92.456	836.44	171.42	1226.7
95.617	845.53	174.49	1246.5
98.663	858.01	177.54	1269.3
101.65	836.03	180.56	1286.8
104.55	838.38	183.57	1317.5
107.58	851.76	186.55	1324.2
110.75	856.35	189.51	1379.3
113.85	883.55	192.45	1419.2
116.90	902.67	195.36	1484.5
119.90	899.37	198.25	1551.8
122.85	914.12	201.25	1629.8
125.76	937.72	204.38	1691.1
128.80	957.17	207.47	1735.5
131.98	974.54	210.55	1783.8
135.12	985.93	213.61	1848.4
138.22	1016.1	216.64	2003.5
141.28	1040.7	219.64	2245.2
144.31	1056.2	222.64	2331.9
147.31	1075.5	225.65	2411.0
150.28	1087.9	228.57	2473.9
153.22	1114.6	231.57	2560.0
156.14	1124.2	234.74	2684.5
159.18	1146.5	237.76	2591.7
240.74	3343.3	316.64	2090.0
243.76	4114.4	319.64	2295.0
246.28	19576	322.56	2317.0
249.65	2161.1	325.55	2497.4
253.43	1985.8	328.50	2592.8
256.30	1996.1	331.44	2681.8
259.28	1973.2	334.36	2779.2
262.18	2009.5	337.29	2870.6
265.02	2016.8	340.32	2951.5
268.05	1940.3	343.34	3038.9
271.11	1908.9	346.36	3153.1
274.19	1880.4	349.48	3272.3
277.26	1902.9	352.60	3384.4
280.36	1899.7	355.71	3517.2
283.36	1958.3	358.80	3656.9
286.42	2079.5	361.89	3795.1
289.45	2277.8	364.96	4015.4
292.44	2523.8	368.01	4326.2
295.45	2073.4	371.03	4834.4
298.46	2113.0	374.08	3379.4
301.46	2155.9	377.25	3343.1
304.49	2072.5	380.41	3319.7
307.51	2050.9	383.58	3334.3
310.53	2025.4	386.76	3322.9
313.57	2042.0		

three peaks from 230 to 390 K on the curve. They were deduced to be the phase transition ($T_{trs} = 246.28$ K), ice point of the free water ($T_{trs} = 292.44$ K), and decompounding of the water ($T_{trs} = 371.03$ K), in the sequence of temperature increments, respectively. The conclusions were made not only experientially, but also based on the DSC measurement and the articles [20–24].

The values of the experimental heat capacities in the three regions can be fitted and four polynomial equations were obtained by least squares fitting using the experimental molar heat capacities ($C_{p,m}$) and the experimental temperatures (T).

- from 80 to 204 K

$$C_{p,m}/(\text{J K}^{-1}\text{ mol}^{-1}) = 1039.4 + 420.07x - 58.086x^2 - 354.31x^3 + 378.97x^4 + 417.07x^5 - 131.1x^6 \quad (1)$$

where $x = [(T/\text{K}) - 142]/(T/\text{K}) - 142]62.62$, x is the reduced temperature, and T is the experimental temperature. Correlation coefficient R^2 of least squares fitting is 0.9999.

- from 252 to 276 K

$$C_{p,m}/(\text{J K}^{-1}\text{ mol}^{-1}) = 2022.7 - 47.434x - 777.69x^2 - 56.203x^3 + 2227.7x^4 + 24.545x^5 - 1803.3x^6 \quad (2)$$

where $x = [(T/\text{K}) - 264]/(T/\text{K}) - 264]12.12$, its correlation coefficient R^2 is 0.9989.

- from 296 to 316 K

$$C_{p,m}/(\text{J K}^{-1}\text{ mol}^{-1}) = 2056.41 - 56.806x + 240.1x^2 - 672.03x^3 - 360.02x^4 + 210.4x^5, \quad (3)$$

where $x = [(T/K) - 306]/(T/K) - 306]10.10$, its correlation coefficient R^2 is 0.9998.

- from 375 to 387 K

$$C_{p,m}/(\text{J K}^{-1}\text{ mol}^{-1}) = 3321.4 + 23.015x + 47.008x^2 - 72.259x^3 \quad (4)$$

where $x = [(T/K) - 381]/(T/K) - 381]6.6$, its correlation coefficient R^2 is 0.9998.

In terms of the polynomials of heat capacity and the thermodynamic relationship, the thermodynamic functions $[H_T - H_{298.15}]$ and $[S_T - S_{298.15}]$ of the complex are calculated in the temperature range from 80 to 390 K with a temperature interval of 5 K and are listed in Table 2.

Table 2 Thermodynamic functions, $[H_T - H_{298.15}]$ and $[S_T - S_{298.15}]$, of the complex from 80 to 390 K at a temperature interval of 5 K

T/K	$C_{p,m}$/ J mol^{-1} K^{-1}	$(H_T - H_{298.15})$/ kJ mol^{-1}	$(S_T - S_{298.15})$/ J mol^{-1} K^{-1}
80	746.35	−207.71	−1246.8
85	797.08	−203.84	−1199.9
90	824.06	−199.78	−1153.6
95	837.79	−195.62	−1108.6
100	845.96	−191.41	−1065.3
105	853.91	−187.16	−1023.8
110	864.97	−182.87	−983.81
115	880.92	−178.50	−945.03
120	902.26	−174.05	−907.16
125	928.60	−169.47	−869.87
130	958.90	−164.75	−832.93
135	991.8	−159.88	−796.15
140	1025.8	−154.83	−759.45
145	1059.6	−149.62	−722.81
150	1092.0	−144.24	−686.27
155	1122.5	−138.70	−649.90
160	1151.3	−133.02	−613.76
165	1178.9	−127.19	−577.91
170	1207.1	−121.23	−542.34
175	1238.4	−115.11	−506.97
180	1276.1	−108.83	−471.63
185	1324.6	−102.33	−436.05
190	1389.3	−95.554	−399.85
195	1476.3	−88.398	−362.58
200	1592.6	−80.735	−323.74
205–250	Phase change	–	–
255	2022.6	−40.675	−152.67
260	1979.1	−30.714	−114.09
265	2013.4	−20.664	−75.806
270	1909.4	−10.868	−39.187
275	1801.4	−1.2511	−4.2700
280–295	Phase change	–	–
298.15	2076.5	0.0000	0.0000
300	2181.3	3.9722	13.279
305	2065.1	14.591	48.388
310	2032.3	24.840	81.720
315	2188.4	35.053	114.40
320–370	Phase change	–	–
375	3417.7	85.983	251.67
380	3319.2	102.72	296.02
385	3336.2	119.37	339.53

DSC analysis

It can be seen from Fig. 2 that there are three endothermic processes in the temperature range from 100 to 300 K, which conforms to the results of the heat capacity measurements. The temperature ranges and peak values of the three endothermic processes correspond to those of the three phase transitions in $C_{p,m} - T$ curve obtained from the heat capacity measurements. It also confirms that there are glass transition and two phase transitions in the temperature range from 150 to 400 K, which include a glass transition, a fusion and a phase transition of the crystalline water.

Based on the DSC curve of Fig. 2, the temperature, T_{trs}, molar enthalpies, $\Delta_{trs}H_m$, and molar entropies, $\Delta_{trs}S_m$ of the phase transitions are determined by the method of diagrammatic area integration and listed in Table 3, being consistent with the values from the heat capacity measurements.

Figure 3 showed that there are two peaks on the DSC curve from 300 to 700 K. One ($T_{trs} = 485$ K) is a little endothermic peak which was coursed by decomposition of amino, the other is a wide exothermic peak from 550 to 600 K which was contributed to decompounding of the complex.

Glass transition and phase transition

Yukawa et al. [21] found a phase transition of the first order and a glass transition of crystalline $(TMA)_2[Sm\{Ni(pro)_2\}_6](ClO_4)_4$ at (190 ± 1) K and (162 ± 2) K. They contributed the phase transition to orientational order/disorder process of perchlorate ions ClO^{4-} and the glass transition to a freezing-in phenomenon of the reorientational motion of perchlorate ions ClO^{4-}. The entropy of the phase

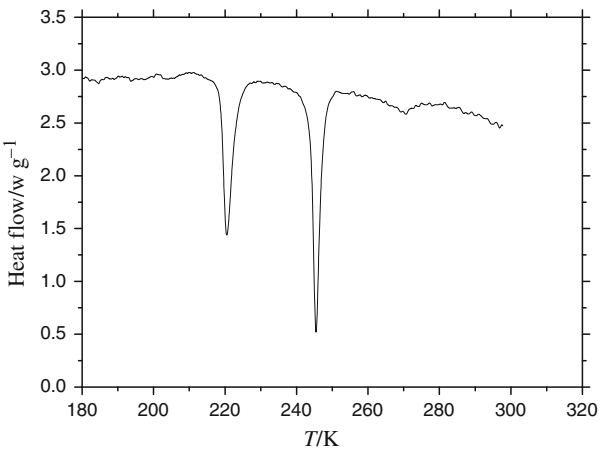

Fig. 2 DSC curve of the complex in the temperature range from 100 to 300 K

Table 3 Temperature, enthalpy and entropy of the phase transitions of the complex obtained from DSC measurement from 150 to 300 K, consistent with the values from the heat capacity measurements (the data in the bracket)

Transition	T_{trs}/K	$\Delta_{trs}H_m$/ kJ mol^{-1}	$\Delta_{trs}S_m$/ J mol^{-1} K^{-1}
Glass transition	220.44 (219.64)	16.98	77.07
Phase transition	245.45 (246.28)	23.07	93.99

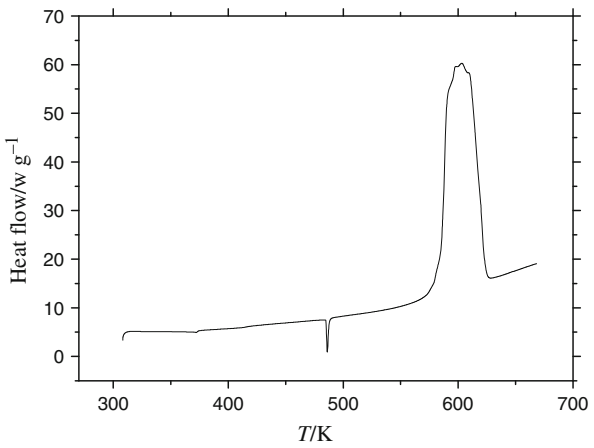

Fig. 3 DSC curve of the complex in the temperature range from 300 to 700 K

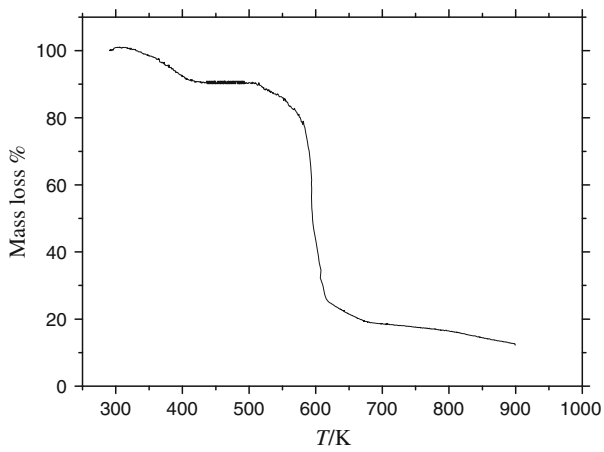

Fig. 4 TG-DTG curve of the complex

transition was estimated to be in the range from 20 to 45 J K^{-1} mol^{-1} and the activation energy for the motion was estimated to be (53 ± 1) kJ mol^{-1}. They discussed that the cooperative interaction between the orientations of the ClO^{4-} ions operates through the orientational and positional shifts of TMA ions, and thus the lattice deformation in the relevant region, associated with the orientational change of the ClO_4^- ions. The position of the ClO^{4-} ions itself would shift to form preferable ionic interaction.

There is a slight step at 219.64 K on the $C_{p,m} - T$ curve of Fig. 1, and a sharp endothermic peak on the DSC curve (Fig. 2) at 220.44 K. The combined consideration of the mechanism of the glass transition, the disappearance of the excess heat capacity and the former documents leads to a conclusion that the phase transition is attributed to glass transition, which was interpreted as a freezing-in phenomenon of the reorientational motion of perchlorate ions ClO^{4-}. The endothermic process at 246.28 K was deduced to be phase transition. The orientational order/disorder process of ClO^{4-} ion is the origin of the phase transition [20–24].

TG analysis

It was showed in Fig. 4 that mass loss of $Er_2(Asp)_2(Im)_8(ClO_4)_6 \cdot 10H_2O$ began at about 298 K and ended at about 900 K. The whole process was divided into three stages. The mechanism of the decomposition was deduced to be

$$Er_2(Asp)_2(Im)_8(ClO_4)_6 \cdot 10H_2O \xrightarrow{\frac{300-429\ K}{9.34\%\ (9.36\%)}} Er_2(Asp)_2(Im)_8(ClO_4)_6 \xrightarrow{\frac{429-584\ K}{14.08\%\ (14.24\%)}} Er_2(Im)_8(ClO_4)_6 \xrightarrow{\frac{559-675\ K}{57.01\%\ (57.15\%)}} Er_2O_3$$

Conclusions

In conclusion, a complex, $Er_2(Asp)_2(Im)_8(ClO_4)_6 \cdot 10H_2O$, which has never been reported, was synthesized and characterized. The heat capacities of the complex were measured and the thermodynamic functions $[H_T - H_{298.15}]$ and $[S_T - S_{298.15}]$ were derived in the temperature range from 80 to 390 K with temperature interval of 5 K. Two thermal events were found at 219.64 and 246.28 K by the AC and DSC techniques, which were interpreted as glass transition and phase change, respectively. Based on the documents, the glass transition was deduced to be the freezing-in phenomenon of the reorientational motion of ClO^{4-} ions and the phase transition was attributed to the orientational order/disorder process of ClO^{4-} ions.

Acknowledgements This study was financially supported by the National Nature Science Foundation of China under the NSFC Grant No. 21003069, 21073189.

References

1. Anghileri LJ. On the antitumor activity of gallium and lanthanides. Arzneim Forsch. 1975;25:793–5.
2. McCarthy GJ. Rare earths in modern science and technology, vol 2. New York: Plenum press; 1980; p. 25–105.

3. Sudhindra NM, Joshi GK, Bhutra MP. Syntheses and absorption spectral studies of Praseodymium (II) and Neodymium (II) complexes with amino acids. Indian J Chem. 1982;21A:275–8.
4. Xu H, Chen L. Study on the complex site of L-tyrosine with rare-earth element Eu^{3+}. Spectrochim Acta A. 2003;59:657–62.
5. Zhang H, Feng J, Zhu W-f. Rare-earth element distribution characteristics of biological chains in rare-earth element-high background regions and their implications. Biol Trace Elem Res. 2000;73:19–27.
6. Glowiak T, Legendziewicz J, Huskowska E, Gawryszewska P. Ligand chirality effect on the structure and its spectroscopic consequences in $[Ln_2(Ala)_4(H_2O)_8](ClO_4)_6$. Polyhedron. 1996;15: 2939–47.
7. Liu B-P, Lv X-C, Tan Z-C, Zhang Z-H, Shi Q, Yang L-N, Xing J, Sun L-X, Zhang T. Molar heat capacity and thermodynamic properties of crystalline $Ho(Asp)Cl_2{\cdot}6H_2O$. J Therm Anal Calorim. 2007;89:283–7.
8. Liu B-P, Tan Z-C, Lu J-l, Lan X-Z, Sun L-X, Xu F, Yu P, Xing J. Low-temperature heat capacity and thermodynamic properties of crystalline $[RE\ (Gly)_3(H_2O)_2]Cl_3{\cdot}2H_2O$ (RE = Pr, Nd, Gly = Glycine). Thermochim Acta. 2003;397:67–73.
9. Qi Y-n, Zhang J, Qiu S-j, Sun L-x, Xu F, Zhu M, et al. Thermal stability, decomposition and glass transition behavior of PANI/NiO composites. J Therm Anal Calorim. 2009;98:533–7.
10. Song L-F, Jiang C-H, Zhang J, Sun L-X, Xu F, et al. Heat capacities and thermodynamic properties of a novel mixed-ligands MOFs. J Therm Anal Calorim. 2010;100:679–84.
11. Song L-F, Jiang C-H, Zhang J, Sun L-X, Xu F, et al. Heat capacities and thermodynamic properties of MgBTC. J Therm Anal Calorim. 2010;101:365–70.
12. Nakamoto K. Infrared spectra of inorganic and coordination compounds. 4th ed. New York: Wiley; 1986. p. 258.
13. Wayda AL, Kaplan ML. Mixed ligand imidazole complexes of organolanthanides. Polyhedron. 1990;9:751–6.
14. Tan Z-C, Liu B-P, Yan J-B, Sun L-X. A fully automated adiabatic calorimeter workable between 80 and 400 K. Comput Appl Chem. 2003;20:264–8. (in Chinese).
15. Nan Z-D, Tan Z-C. Low-temperature heat capacities and derived thermodynamic functions of cyclohexane. J Therm Anal Calorim. 2004;76:955–63.
16. Tong B, Tan Z-C, Lv X-C, Sun L-X, Xu F, Shi Q, Li Y-S. Low-temperature heat capacities and thermodynamic properties of 2,2-dimethyl-1,3-propanediol. J Therm Anal Calorim. 2007;901: 217–21.
17. Lv X-C, Gao X-H, Tan Z-C. Molar heat capacity and thermodynamic properties of 1,2-cyclohexane dicarboxylic anhydride $[C_8H_{10}O_3]$. J Therm Anal Calorim. 2008;92:523–7.
18. Tan Z-C, Sun G-Y, Yin A-X, Wang W-B, Ye J-C, Zhou L-X. An adiabatic low-temperature calorimeter for heat capacity measurement of small samples. J Therm Anal. 1995;45:59–67.
19. Donald GA. Thermodynamic properties of synthetic sapphire standard reference material 720 and the effect of temperature-scale difference on thermodynamic properties. J Phys Chem Ref Data. 1993;22:1441–52.
20. Anna MM, Edward M, Hetmańczyk L, Natkaniec I, Ściesińska E, Ściesiński J, Wróbel S. Phase transition, molecular motions, structural changes and low-frequency vibrations in $[Cu(NH_3)_5](ClO_4)_2$. Chem Phys. 2005;317:188–97.
21. Hangam SS, Westrumj ER. Heat capacities and thermodynamic properties of globular molecules. I. Adamantane and hexamethylenetetramine. Thermodyn Prop Globul Mol. 1960;64:1547–51.
22. Yukawa Y, Igarashi S, Masuda Y, Oguni M. Phase transition and glass transition concerning configurational order/disorder of ions in crystalline $(TMA)_2[Sr\{Ni(pro)_2\}_6](ClO_4)_4$ and $(TMA)[Sm\{Ni(pro)_2\}_6](ClO_4)_4$. J Mol Struct. 2002;605:277–90.
23. Udowenko AA, Laptash NM, Maslennikova IG. Orientation disorder in ammonium elpasolites: crystal structures of $(NH_4)_3AlF_6$,$(NH_4)_3TiOF_5$ and $(NH_4)_3FeF_6$. J Fluor Chem. 2003;124: 5–15.
24. Meng J-X, Li J-H, Xie G-W, Huang W-G, Liang H-Z. Lanthanide ion luminescence probe: low temperature phase transition of EuS_4N complex. Spectrosc Spectr Anal. 2002;22:562–5. (in Chinese).